TOPICAL REVIEW — Magnetism, magnetic materials, and interdisciplinary research

Martensitic transformation and related magnetic effects in Ni–Mn-based ferromagnetic shape memory alloys*

Wang Dun-Hui(王敦辉)†, Han Zhi-Da(韩志达), Xuan Hai-Cheng(轩海成), Ma Sheng-Can(马胜灿), Chen Shui-Yuan(陈水源), Zhang Cheng-Liang(张成亮), and Du You-Wei(都有为)

National Laboratory of Solid State Microstructures, Department of Physics, Nanjing University, Nanjing 210093, *China*

(Received 3 May 2013)

Ferromagnetic shape memory alloys, which undergo the martensitic transformation, are famous multifunctional materials. They exhibit many interesting magnetic properties around the martensitic transformation temperature due to the strong coupling between magnetism and structure. Tuning magnetic phase transition and optimizing the magnetic effects in these alloys are of great importance. In this paper, the regulation of martensitic transformation and the investigation of some related magnetic effects in Ni–Mn-based alloys are reviewed based on our recent research results.

Keywords: magnetocaloric effect, magnetoresistance effect, exchange bias, magnetoelectric effect

PACS: 75.30.Kz, 75.30.Sg, 75.50.Cc, 75.47.De **DOI:** 10.1088/1674-1056/22/7/077506

1. Introduction

Ferromagnetic shape memory alloys (FSMAs), which exhibit ferromagnetism and a shape memory effect simultaneously, have attracted more and more attention for their potential applications in many areas. They exhibit many interesting magnetic properties around the martensitic transformation temperature due to the strong coupling between magnetism and structure. Upon cooling, they undergo a first-order magnetostructural transition from a parent austenitic phase to a martensitic phase, with abrupt changes of magnetization and lattice constants. The first FSMAs discovered are near-stoichiometric Ni_2MnGa Heusler alloys, in which a giant magnetostrain effect is observed due to the magnetically induced twin boundary motion in the martensitic phase.[1–3] Besides this property, a large magnetocaloric effect (MCE) was reported in $Ni_{51.5}Mn_{22.7}Ga_{25.8}$ alloy by Hu *et al.* at the Institute of Physics, Chinese Academy of Sciences, which extends the application field of this FSMA as a potential candidate for magnetic refrigeration.[4] In 2004, Sutou *et al.* found some new FSMAs, Ni–Mn–Z (Z = In, Sn, Sb) alloys, in which the martensitic transformation (MT) was observed in their off-stoichiometric systems.[5] Since the magnetostructural transition in these FSMAs can be induced by an external magnetic field, some magnetic-transition-related effects (MTREs), such as magnetocaloric, magnetoresistance, and magnetostrain effects, are obtained in Ni–Mn–Z alloys.[6–8] More and more attention is therefore paid to these multifunctional materials for promising applications. Both the tuning of the magnetic phase transition and the optimization of the magnetic effects in these alloys have taken on special importance.

FSMAs can be regarded as the combination of ferromagnetic (FM) martensite and parent phases, and the MT is generally observed between the FM (or paramagnetic (PM)) martensite phase and the FM (or PM) austenite phase due to the inequality of their magnetostructural phase transition temperatures. According to the Clausius–Clapeyron relation in the magnetic phase diagram, making MT occur between the PM martensite phase and the FM parent phase in Ni–Mn-based FSMAs helps to decrease the driving magnetic field and gain large MTREs.[8] On the other hand, FSMAs exhibit large effects only in the vicinity of the phase transition temperature, which markedly limits their applications. From the application point of view, tuning MT and making FSMAs exhibit large MTREs at a low magnetic field and desired temperature regions is greatly desired. In this paper, we review our recent progress in the regulation of MT and the investigation of some MTREs in Ni–Mn-based FSMAs.

2. Structure and magnetism in Ni–Mn-based FSMAs

The prototype Ni–Mn-based FSMA, an alloy composed of the 2–1–1 Heusler stoichiometry and Ni_2MnGa, is the only system with stoichiometric composition that undergoes the MT. In the austenite state, the Ni_2MnGa Heusler alloy has an $L2_1$ structure (space group $Fm3m$), which consists of four interpenetrating face-centered cubic (fcc) sublattices.[9] With decreasing temperature, it undergoes an MT and acquires a number of structures of martensite phases, such as the 5M and

*Project supported by the National Basic Research Program of China (Grant No. 2012CB932304) and the National Natural Science Foundation of China (Grant No. U1232210).

†Corresponding author. E-mail: wangdh@nju.edu.cn

© 2013 Chinese Physical Society and IOP Publishing Ltd

the 7M modulated structures. But in the case of Ni–Mn–*Z* FSMAs, the MT can be observed only in their off-stoichiometric compositions, and mainly in Mn-rich alloys.[5] With the substitution of Mn for *Z* atoms, the excess Mn atoms occupy the *Z* sites and the moments are coupled antiferromagnetically to those of the surrounding Mn atoms on the regular Mn sites. In the Ni–Mn-based FSMAs, the magnetic moments are confined to the Mn atoms to a large extent and the magnetic properties can often be described in terms of localized magnetic moments with indirect exchange interactions, despite the fact that they are metals.[9,10] Figure 1 shows the typical thermomagnetization curves for Ni–Mn–Cr–Sn FSMAs on cooling and heating.[11] The characteristic temperatures of FSMSs are the martensitic start temperature M_s, martensitic finish temperature M_f, austenitic start temperature A_s, austenitic finish temperature A_f, and Curie temperatures of the martensitic phase T_C^M and austenitic phase T_C^A. Upon heating, the FM behavior is observed in the martensitic state at first, and then magnetization decreases with increasing temperature. Further increasing the temperature causes a sudden jump of magnetization, corresponding to the reverse MT. Then the austenite state undergoes a transition from FM phase to PM phase. An obvious thermal hysteresis between the cooling and heating processes is observed in Fig. 1, suggesting that the MT is a first-order transition.

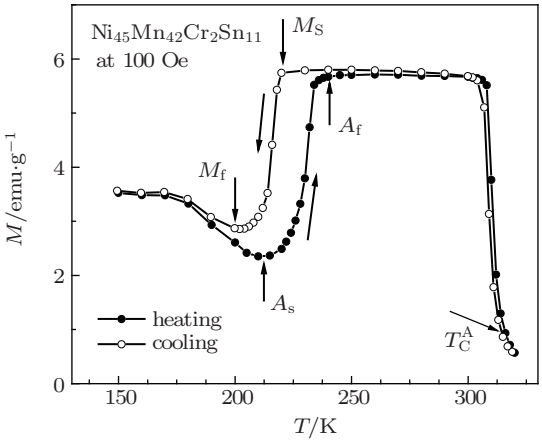


Fig. 1. Typical thermomagnetization curves for Ni–Mn–Cr–Sn FSMAs on cooling and heating at 100 Oe.[11]

3. Regulation of MT in Ni–Mn–*Z* FSMAs

3.1. Tuning valence electron concentration

In Ni–Mn-based FSMAs, the change of chemical composition can alter the electronic structure and the number of conducting electrons, and then affect the MT through the modification of electron density and exchange interaction.[9,10] Accordingly, it is reported that the MT temperatures of these alloys are very sensitive to the valence electron concentration e/a (electrons per atom). Here the number of valence electrons is calculated as the number of 3d and 4s electrons of a 3d-transition metal and the number of 5s and 5p electrons of a *Z* atom.[10] Therefore, tuning the chemical composition is an effective method to adjust the MT of Ni–Mn–*Z* alloys.

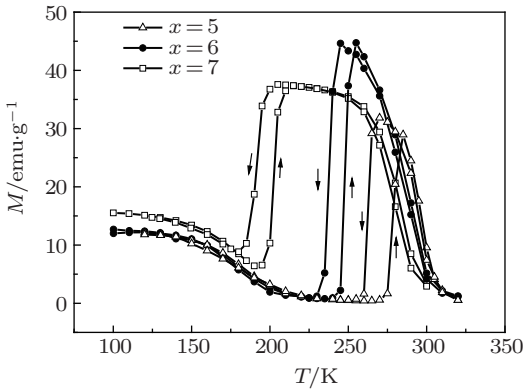


Fig. 2. Temperature dependence of magnetization for $Ni_{50-x}Mn_{39+x}Sn_{11}$ alloys ($x = 5, 6, 7$).[12]

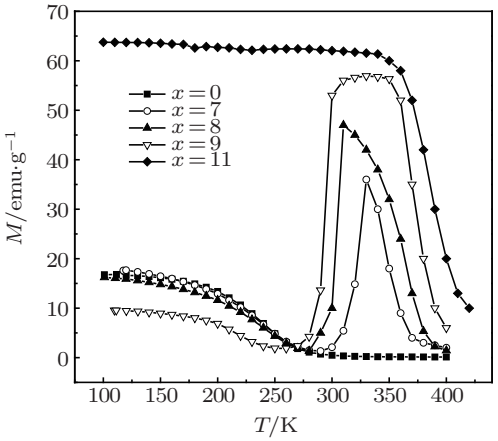


Fig. 3. Temperature dependence of magnetization for $Ni_{50-x}Co_xMn_{39}Sb_{11}$ alloys ($x = 0, 7, 8, 9, 11$).[13]

Figure 2 shows the temperature dependence of magnetization (M–T) for $Ni_{50-x}Mn_{39+x}Sn_{11}$ alloys, in which a remarkable change of MT temperature is observed due to the change of Ni/Mn ratio.[12] As for the substitution method, using other 3d elements, such as Cr, Co, and Cu, to substitute for Ni or Mn has also proven to be a useful way to change the MT temperature.[11,13,14] Figures 3 and 4 show the M–T curves for Ni–Mn–Co–Sn and Ni–Mn–Cu–Sb alloys, respectively. It is obvious that the MT temperatures decrease (increase) with increasing Co (Cu) contents, corresponding to the decrease (increase) of the e/a values. In order to obtain a large change of magnetization (ΔM) between the martensitic and austenitic phases, the criterion $T_C^M < M_s < T_C^A$ should be satisfied. As shown in Fig. 3, large values of ΔM are observed in the alloys of $x = 7, 8, 9$. As for $Ni_{39}Co_{11}Mn_{39}Sb_{11}$, besides the FM transition at T_C^A, no obvious MT can be identified in the M–T curve, since M_s is lower than T_C^M. Unlike the aforementioned doping methods with 3d-transition metal elements, Han *et al.* reported the investigation of MT in $Mn_{50}Ni_{50-x-y}Nb_xSn_y$ alloys, in which a 4d-transition metal element is substituted for Ni.[15] Figure 5 shows the characteristic temperatures of phase

transitions as a function of Nb content and e/a value for those FSMAs. Obviously, the values of M_s, M_f, A_s, and A_f decrease with the increase of Nb content due to the decrease of e/a value. For the Curie temperatures, with increasing Nb content, T_C^M remains almost a constant, while T_C^A shows a slight decrease, suggesting that the influence of Nb on the exchange interaction is small.[15]

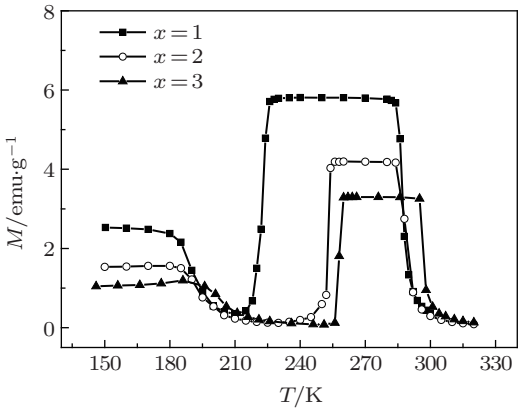


Fig. 4. Temperature dependence of magnetization for $Ni_{43}Mn_{46-x}Cu_xSn_{11}$ alloys ($x = 1, 2, 3$).[14]

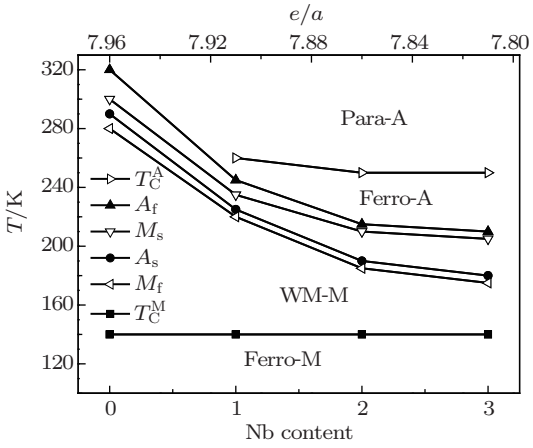


Fig. 5. Characteristic temperatures of phase transitions as a function of Nb content and e/a value for $Mn_{50}Ni_{50-x-y}Nb_xSn_y$ alloys.[15]

3.2. Modifying Mn–Mn distance

Since the magnetic moments are confined to the Mn atoms and the occupation of Mn atoms affects the exchange interaction, the interatomic distance between Mn atoms plays a key role in determining the magnetostructural transition of Ni–Mn-based FSMAs. Actually, the substitution of other elements for Ni, Mn, or Z atoms changes not only the valence electron concentration but also the cell volume, both of which would affect the MT of Ni–Mn–Z alloys. As for the isoelectronic substitution, for example in $Ni_{50}Mn_{34}In_{16-x}Ga_x$[16] and $Ni_{43}Mn_{46}Sn_{11-x}Ge_x$[17] alloys, Ga or Ge has the same number of valence electrons as In or Sn, respectively. Thus, in these cases, the effect of e/a on the MT should be neglected and the variation of the Mn–Mn distance caused by doping elements with different ionic radii should be taken into account. Figure 6 shows the M–T curves for $Ni_{43}Mn_{46}Sn_{11-x}Ge_x$ alloys in a magnetic field of 1 kOe on heating and cooling, in which an obvious decrease of the MT temperature is observed with increasing Ge content. In $Ni_{43}Mn_{46}Sn_{11-x}Ge_x$ alloys, due to the smaller ionic radius of Ge, the decrease of the cell volume would result in the decrease of the Mn–Mn distance, and as a consequence, decrease the MT temperature. It is noted that T_C^A also changes markedly with the variation of the Ge content, suggesting the effect of the Mn–Mn distance on the exchange interaction of austenitic phase.

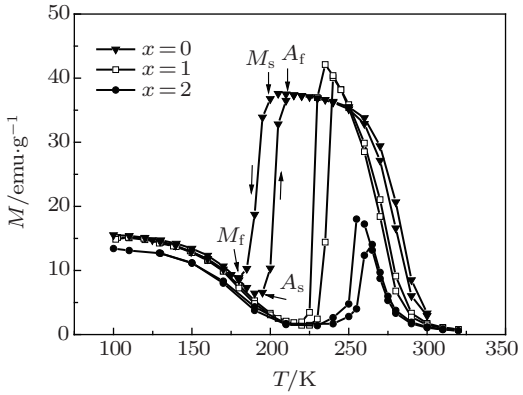


Fig. 6. The M–T curves for $Ni_{43}Mn_{46}Sn_{11-x}Ge_x$ ($x = 0, 1, 2$) alloys in a magnetic field of 1 kOe on heating and cooling.[17]

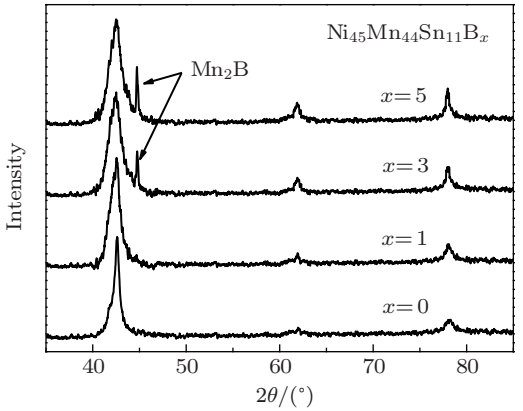


Fig. 7. X-ray diffraction patterns for $Ni_{43}Mn_{46}Sn_{11}B_x$ ($x = 0, 1, 3, 5$) alloys obtained at room temperature.[19]

It is reported that introducing interstitial atoms with a small atomic radius, such as carbon or hydrogen atoms, is a useful method to tune the magnetic phase transition temperature by modifying the distance between magnetic ions.[18] Based on this mechanism, the investigation of MT was performed in a series of $Ni_{43}Mn_{46}Sn_{11}B_x$ alloys, in which boron acts as an interstitial atom.[19] Figure 7 shows the X-ray diffraction patterns of B-doped alloys obtained at room temperature. It is obvious that these alloys retain the $L2_1$-type structure after the introduction of boron atoms. With the increase of the boron content, a foreign phase of Mn_2B appears. The lattice constants of the alloys are 5.978 Å, 5.981 Å,

5.984 Å, and 5.986 Å for x=0, 1,3, and 5, respectively. Figure 8 presents the M–T curves for all $Ni_{43}Mn_{46}Sn_{11}B_x$ alloys on heating in a magnetic field of 100 Oe. Obviously, the transformation temperatures, including the characteristic temperatures of MT and T_C^A of $Ni_{43}Mn_{46}Sn_{11}B_x$ alloys, increase with the increasing boron content, which is attributed to the change of the Mn–Mn distance caused by the interstitial introduction.[19]

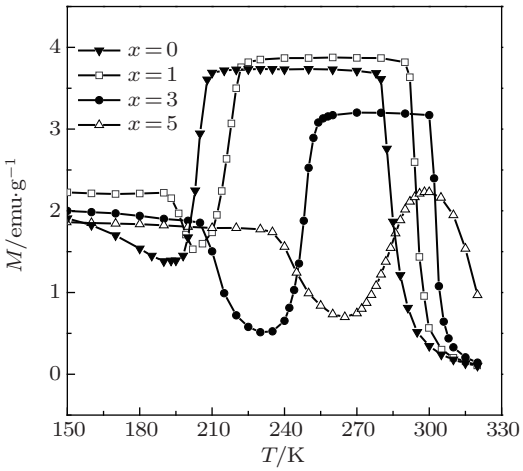


Fig. 8. The M–T curves for all $Ni_{43}Mn_{46}Sn_{11}B_x$ alloys on heating in a magnetic field of 100 Oe.[19]

3.3. Altering internal or external stress

It is well known that the MT of Ni–Mn-based FSMAs can be driven not only by temperature and magnetic field, but also by stress, which is a distinctive property of these multifunctional materials. Applying stress on Ni–Mn–Z alloys can modify the Mn–Mn distance and affect the relative stability between the high temperature cubic phase and the low temperature martensitic phase, thereby affecting the magnetostructural transition. It has been reported that a hydrostatic pressure has a remarkable effect on the MT in many Ni–Mn-based FSMAs, such as Ni–Mn–In, Ni–Mn–Co–Sb, and nickel-rich Ni–Mn–Ga alloys.[10,20,21] We all know that pre-deformation can increase the MT temperature in some shape memory alloys (such as TiNi, TiNiNb), as has been verified by thermal and electrical measurements.[22–24] Accordingly, Ma *et al.* reported the effect of pre-pressure on the MT in Ni–Mn–Co–Sn ribbons.[25] Figure 9 shows the M–T curves for melt-spun ribbons and pre-deformed ribbons, compressed under 1.05 GPa and 1.95 GPa, upon heating. It is observed that the MT temperature increases with increasing pressure, suggesting that the relative stability between the parent and the martensitic phases can be affected by pre-deformation. On the other hand, due to the lower volume of the martensitic phase in contrast to the cubic phase, the pre-pressure would favor the martensitic phase from the thermodynamic point of view and support the martensite to a higher temperature, which is also responsible for the increase of the MT temperature. As shown in Fig. 9, there is no significant enhancement of T_C^A, indicating that the pre-deformation has little effect on the second-order magnetic phase transition of the high temperature parent phase.[25]

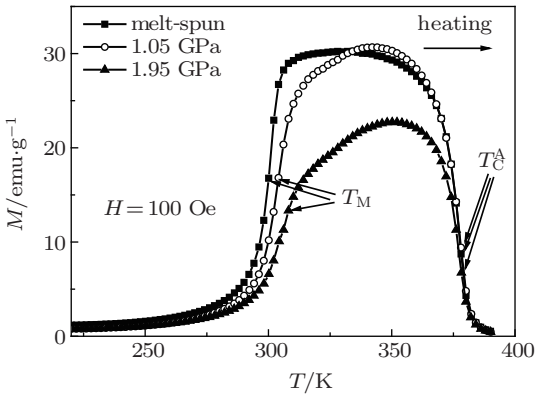


Fig. 9. The M–T curves for melt-spun Ni–Mn–Co–Sn ribbons and pre-deformed Ni–Mn–Co–Sn ribbons compressed under 1.05 GPa and 1.95 GPa at 100 Oe on heating.[25]

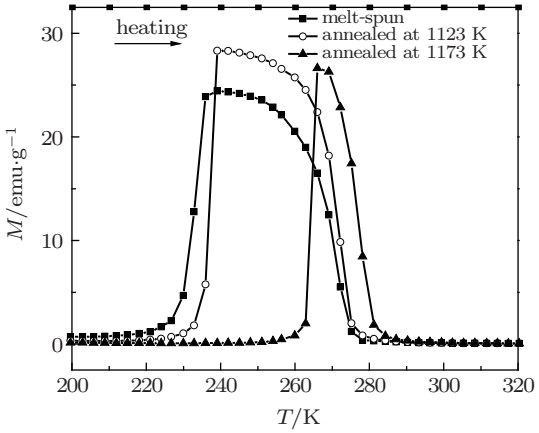


Fig. 10. The M–T curves under a magnetic field of 100 Oe for the melt-spun and annealed Ni–Mn–Sn ribbons on heating.[28]

Rapid quenching by melt spinning is reported as an effective method to achieve homogeneous Ni–Mn–Z FSMAs, avoiding or at least reducing the time of annealing, and making it easy to obtain highly textured polycrystalline ribbons.[26,27] In this way, melt-spun ribbons have been obtained by rapid cooling from a liquid alloy. They possess a metastable structure and a higher energy, because the atoms, during the quick transition from the liquid to the solid state, do not take up the equilibrium positions with lower energy. Annealing the as-quenched ribbons would modify the short-range order of atoms, thereby affecting the exchange interaction. Based on this mechanism, Xuan *et al.* reported the effect of heat treatment on the MT in Ni–Mn–Sn melt-spun ribbons.[28] The experiment results show that, after the annealing process, the MT temperature increases obviously in the annealed ribbons, as shown in Fig. 10. As mentioned above, there is a residual internal stress in melt-spun Ni–Mn–Sn ribbons due to the rapid cooling. After annealing, the as-quenched ribbons undergo

structural and stress relaxations, which may change the Mn–Mn distance, resulting in the increased MT temperature in Ni–Mn–Sn ribbons. Therefore, altering the internal stress by heat treatment is also an effective way to tune the MT temperature in Ni–Mn-based FSMAs.

3.4. Intermediate phase transition in Ni–Mn–Sn alloys

Ni–Mn–Ga Heusler alloys have been extensively investigated as prototypical FSMAs. More interestingly, some of these alloys with composition close to the stoichiometric Ni_2MnGa exhibit a weak first-order phase transition from the austenitic phase to the intermediate phase prior to the MT.[29–31] This intermediate phase transition is often characterized by anomalies in the elastic, thermal, resistivity, and magnetic properties. It is widely believed that the intermediate phase transition originates mainly from the magnetoelastic coupling between the magnetic and the structural degrees of freedom in the Ni–Mn–Ga alloy system.[29–31] However, there are very few reports about the intermediate phase in Ni–Mn–Z alloys that were discovered very recently. Considering that the high-pressure synthesis is a useful method to enhance the magetoelastic coupling in magnetic materials, we studied the magnetic phase transitions in an Ni–Mn–Co–Sn alloy prepared by high-pressure annealing (HPA) at 4 GPa.[32] Figure 11 shows the M–T curves for Ni–Mn–Co–Sn melt-spun ribbon and HPA alloy in a field of 100 Oe on heating. It is observed that the MT temperature increases with HPA, indicating the effect of external stress on the phase transition temperature. It is worth noting that an anomaly of the thermomagnetic behavior is observed in the HPA alloy, occurring between MT and the FM transition of austenite. As shown in the inset of Fig. 11, magnetization above MT displays a bump at a temperature around 334 K. The rise in magnetization between A_f and 334 K is somewhat similar to the jump of magnetization observed around the MT, suggesting that the martensitic phase transition should be a two-step process and an intermediate phase may exist in HPA Ni–Mn–Co–Sn alloy.[32] This phase transition can be further verified by the electrical resistance and calorimetric measurements, which are shown in Fig. 12. The application of external stress may induce an enhanced magnetoelastic coupling between the magnetic and the structural degrees of freedom in HPA Ni–Mn–Co–Sn alloy, which would be responsible for the appearance of the intermediate phase.[32]

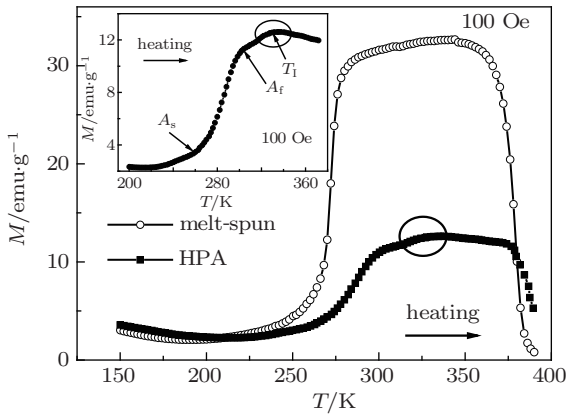


Fig. 11. Temperature dependence of the magnetization for Ni–Mn–Co–Sn melt-spun ribbon and HPA alloy in the field of 100 Oe on heating. The inset presents a partly enlarged view of the M–T curve for the HPA alloy.[32]

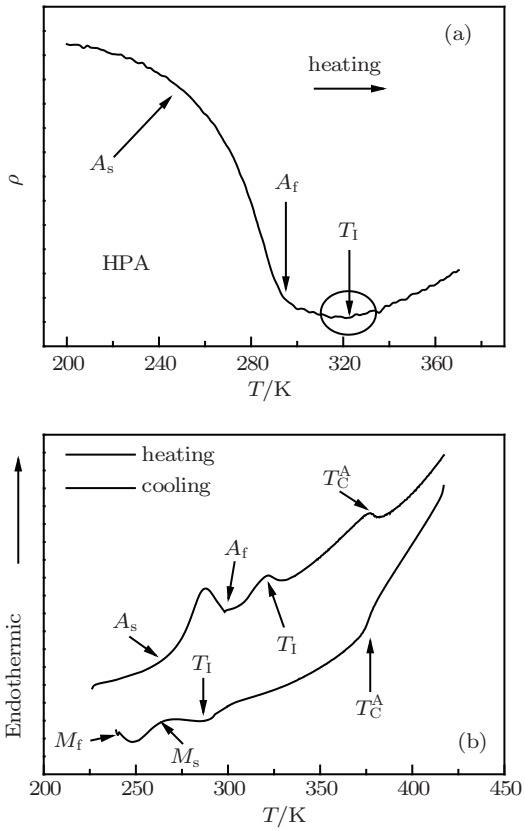


Fig. 12. (a) Variation in the resistivity of HPA alloy versus temperature and (b) DSC curves upon cooling and heating at a rate of 10 K/min for HPA alloy.[32]

4. MT related effects in Ni–Mn–Z alloys

4.1. Magnetocaloric effects

Magnetic materials with a large MCE have attracted increasing attention in recent years for their potential applications as magnetic refrigerants. Compared with the conventional refrigerators based on the compression–expansion of gas, the magnetic refrigerators have many advantages, such as high efficiency, small volume, and freedom from harmful gas leakage. Therefore, magnetic refrigeration is considered to be an environmentally friendly technology.

The Ni–Mn-based FSMAs are reported to exhibit a large MCE due to the large change of magnetization around the magnetic phase transition, which makes them potential candidates for magnetic refrigeration. For a special review about the MCE of FSMAs, readers are referred elsewhere,[9] and

hereafter we just introduce some MCE results from our recent work.

From the application point of view, magnetic refrigeration at room temperature is obviously highly desirable. By tuning the composition, especially substituting Co for Ni or Mn, the MT temperature can be effectively adjusted to room temperature.[13] Figure 13 plots the temperature dependence of magnetic entropy changes ($\Delta S_{\rm M}$) for $Ni_{50-x}Co_xMn_{39}Sb_{11}$ ($x = 7$, 8, 9) alloys at 10 kOe. These FSMAs all show a large MCE at low magnetic fields, and the working temperature of the $Ni_{42}Co_8Mn_{39}Sb_{11}$ alloy is just at the room temperature.[13]

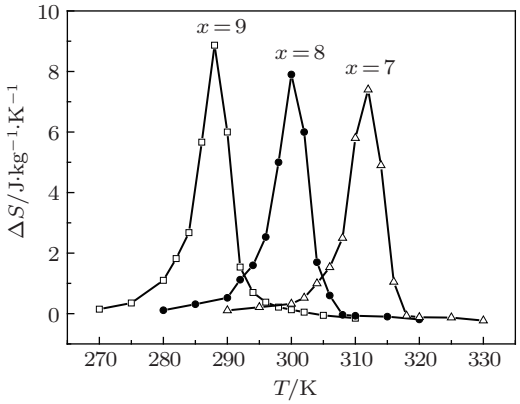


Fig. 13. Temperature dependence of $\Delta S_{\rm M}$ in a magnetic field of 10 kOe for $Ni_{50-x}Co_xMn_{39}Sb_{11}$ alloys.[13]

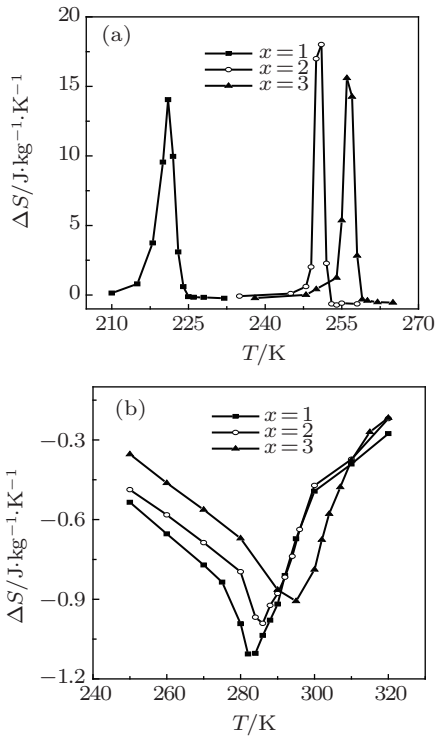


Fig. 14. Temperature dependence of $\Delta S_{\rm M}$ in a magnetic field of 10 kOe for $Ni_{43}Mn_{46-x}Cu_xSn_{11}$ ($x = 1$, 2, 3) around (a) MT temperature and (b) $T_{\rm C}^{\rm A}$.[14]

Besides the magnetostructural transition in Ni–Mn-based FSMAs, there is another second-order FM transition around $T_{\rm C}^{\rm A}$, which also gives rise to the change of magnetic entropy. Therefore, a coexistence of negative and positive MCEs can be observed in these alloys. Figure 14 shows the temperature dependence of MCE for $Ni_{43}Mn_{46-x}Cu_xSn_{11}$ alloys at 10 kOe.[14] The values of $\Delta S_{\rm M}$ around the MT temperature are very large and the MT can be tuned by adjusting the concentration of Cu, which is important for the application of magnetic refrigeration. In the case of MCE around $T_{\rm C}^{\rm A}$, the magnitude of $\Delta S_{\rm M}$ is relatively small, but the refrigeration capacity is large.[14]

For magnetic refrigeration, a wide operating temperature range is of great importance. The HPA Ni–Mn–Co–Sn alloy shows a two-step phase transition process, and as a consequence, two successive positive MCE peaks are observed around room temperature, i.e., 284 K and 320 K, corresponding to the MT and the intermediate phase transition, respectively, which are shown in Fig. 15.[32] As we know, two successive MCE peaks with the same sign have been discovered in some second-order phase transition materials, such as $PrNiCo_5$ and Ho_2In,[33,34] which enlarge the working temperature range effectively. In the case of HPA Ni–Mn–Co–Sn alloy, two $\Delta S_{\rm M}$ peaks with the same sign are partly overlapping as well, giving rise to a wide refrigerant temperature interval of about 67 K with appreciable MCE, which is indicated by the shaded area in Fig. 15.[32]

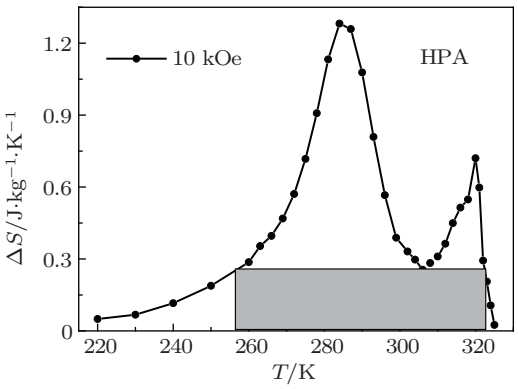


Fig. 15. Temperature dependence of $\Delta S_{\rm M}$ for HPA alloy in a magnetic field of 10 kOe. The shadow area indicates the refrigerant temperature interval.[32]

4.2. Magnetoresistance effect

The Ni–Mn–Z alloys undergo a magnetostructural transition from the high-temperature austenitic phase to the low-temperature martensitic phase with decreasing temperature. Since the crystallographic symmetry changes through the MT, the band structure varies correspondingly, leading to different densities of state near the Fermi level and a sharp change in resistivity near the MT temperatures.

Figure 16 shows the temperature dependence of the electrical resistivity for $Ni_{45}Mn_{42}Cr_2Sn_{11}$ alloy at $H = 0$ and 50 kOe on heating, in which a typical resistivity behavior of Ni–Mn-based FSMA is observed.[11] In the martensite

state, the resistivity decreases with increasing temperature, and around the MT temperature of 230 K, a sudden drop of the resistivity is observed. Further warming leads to the increase of resistivity in the austenite state. It seems that the resistivity exhibits a semimetal-like behavior in the martensitic state, while it is metallic for the austenitic state. As we know, the first-order MT in Ni–Mn-based FSMAs often develops with a region of metastability with austenite and martensite coexisting. With increasing temperature, especially around the MT temperature, more and more martensitic fractions in the sample are transformed into the austenitic phase. Since the martensite phase has higher resistivity as compared with the austenite phase, the overall resistivity decreases with increasing temperature, showing the semimetal-like behavior around the MT temperature despite the metallic nature of martensite and austenite states.[35] In addition, a downshift of 15 K in the MT temperature is observed in $Ni_{45}Mn_{42}Cr_2Sn_{11}$ alloy at 50 kOe, suggesting that the transition from weak-magnetic martensite to FM austenite can be realized in advance with a sufficiently strong applied magnetic field.

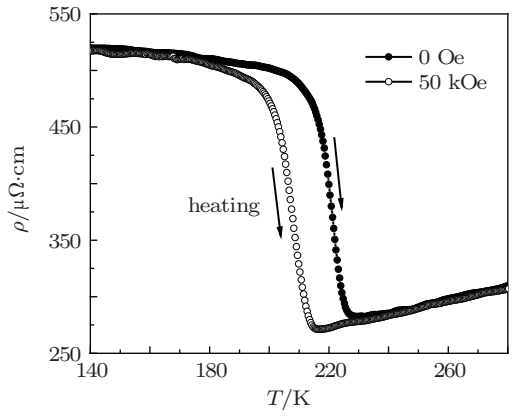


Fig. 16. Temperature dependence of electrical resistivity in the magnetic fields of 0 Oe and 50 kOe for $Ni_{45}Mn_{42}Cr_2Sn_{11}$ alloy.[11]

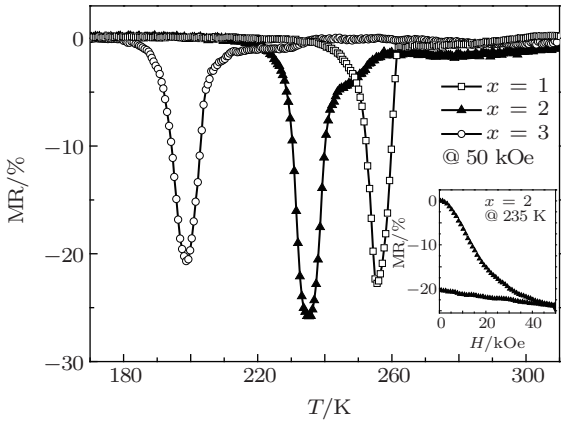


Fig. 17. Temperature dependence of MR for $Mn_{47+x}Ni_{43-x}Sn_{10}$ ($x = 1$, 2, 3) alloys at a magnetic field of 50 kOe. Inset: field dependence of MR for $Mn_{49}Ni_{41}Sn_{10}$ alloy at 235 K.[36]

Since the magnetic field can induce the magnetostructural phase transition in Ni–Mn-based FSMAs, a large magnetoresistance (MR) effect is expected. Figure 17 plots the temperature dependence of MR for the high-Mn content alloys, $Mn_{47+x}Ni_{43-x}Sn_{10}$, at a magnetic field of 50 kOe.[36] The maximum values of MR for $x = 1$, 2, and 3 alloys under the magnetic field of 50 kOe are 23%, 25%, and 21%, respectively. The inset of Fig. 17 shows the magnetic field dependence of MR for the $Mn_{49}Ni_{41}Sn_{10}$ alloy at 235 K. The value of MR decreases gradually with increasing magnetic field and becomes almost saturated under a field of 35 kOe. It is noted that the MR remains almost unchanged as the magnetic field decreases from 50 kOe to 0 Oe, implying that the alloy remains in a kinetically arrested austenite phase and the return transformation from austenite to martensite cannot be realized.[36]

4.3. Exchange bias effect

The exchange bias was discovered at the interface between the FM Co core and the antiferromagnetic (AFM) CoO shell by Meiklejohn and Bean in 1956. From then on, extensive investigations have been carried out on this subject in many systems for its applications in ultrahigh-density magnetic recording, giant magnetoresistance, sensors, and spintronic devices. The exchange bias is usually described as the shift hysteresis loops along the field axis for coupled AFM–FM systems cooled though the Néel temperature in the presence of a magnetic field, which is due to a unidirectional magnetic anisotropy caused by the coupling between the AFM and the FM at the interface. To date, the exchange bias has been investigated in many systems, such as small oxide particles, multilayer films, and inhomogeneous materials.

For Mn rich $Ni_{50}Mn_{25+x}Sn_{25-x}$ Heusler alloys, the excess Mn atoms occupy the Sn sites. In such spatial configurations, the Mn–Mn neighbors have a smaller separation than those in the stoichiometric compound, which would introduce an AF exchange in these off-stoichiometric alloys.[9] It is well known that the coexistence of FM and AFM phases in the martensitic phase and the coupling at the AFM/FM interface result in the exchange bias behavior, which has been observed in some Ni–Mn–Z alloys, such as $Ni_{50}Mn_{25+x}Sb_{25-x}$[37] and $Ni_{50}Mn_{36}Sn_{14}$.[38] However, the exchange bias properties in the alloys with high contents of Mn, especially when the content of Mn is higher than that of Ni, have rarely been investigated. In these alloys, the excess Mn atoms would occupy not only the Sn sites but also the Ni sites, and the moments of Mn at the tetrahedral (Ni) sites are antiparallel to those of Mn atoms at the octahedral (Mn) sites. Through the MT, the Mn–Mn distance decreases due to the twinning of the martensitic phase, leading to the enhanced strength of the AF exchange coupling in Ni–Mn–Sn alloys with high Mn content.[39]

Figure 18 shows the temperature dependence of zero field cooled (ZFC) and field cooled (FC) magnetization curves for $Mn_{50}Ni_{40}Sn_{10}$ alloy.[39] With decreasing temperature, the

PM–FM transition occurs at a T_C^A of about 280 K. Then a sudden decrease in magnetization is observed, corresponding to the transition from austenite to martensite. Further decreasing the temperature leads to an FM transition of the martensitic phase. Below the Curie temperature of the martensite T_C^M, a splitting is observed between the ZFC and FC curves and becomes much more pronounced with decreasing temperature, showing the coexistence of AFM and FM exchange interactions in the martensite state.

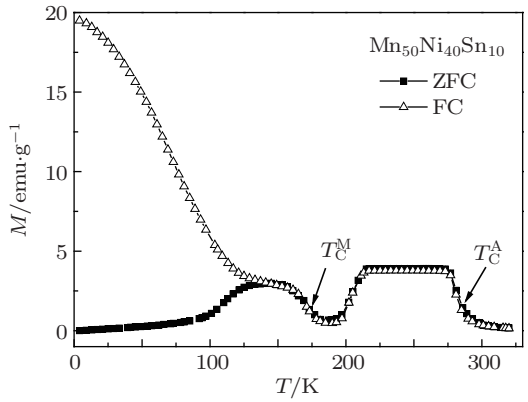


Fig. 18. ZFC and FC magnetization curves as a function of temperature for $Mn_{50}Ni_{40}Sn_{10}$ alloy under a magnetic field of 100 Oe.[39]

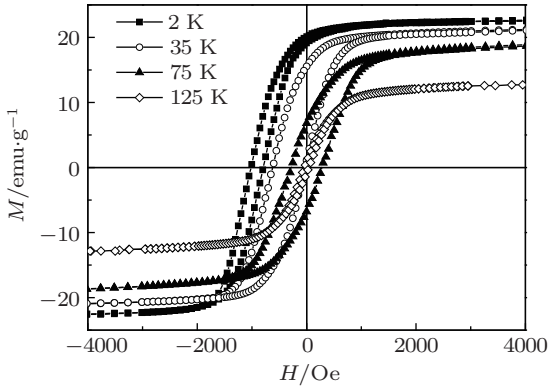


Fig. 19. Magnetic hysteresis loops for $Mn_{50}Ni_{40}Sn_{10}$ alloy measured at different temperatures.[39]

Figure 19 shows the magnetic hysteresis loops of $Mn_{50}Ni_{40}Sn_{10}$ alloy at different temperatures measured after the FC process from 320 K. It is obvious that the magnetization curve at 2 K shifts completely to the negative field axis with a considerably large exchange bias field (H_E) of 910 Oe. Here the value of H_E is calculated using $H_E = -(H_1 + H_2)/2$, where H_1 and H_2 are the left and right coercive fields, respectively. With increasing temperature, the value of H_E decreases and the shift in the hysteresis loop almost disappears at 75 K. Therefore, the temperature of 75 K can be referred as the exchange blocking temperature, T_B, where the AFM cannot pin the FM regions and the FM domains begin to rotate. Above T_B, an asymmetrical hysteresis loop is observed at 125 K. As mentioned above, the excess Mn atoms in high-Mn-content $Mn_{50}Ni_{40}Sn_{10}$ alloy occupy both the Ni and Sn sites and their moments are coupled antiferromagnetically to those of Mn atoms on the regular Mn sites. After the MT, the AFM interaction in the martensitic phase is enhanced due to the change in the Mn–Mn distance, which is strong enough to pin the FM domains. It is worth noting that, unlike the Ni–Mn based FSMAs with high Ni content, another AFM interaction between Mn atoms at the Ni sites and the ones at the regular sites is introduced in the present alloy. Consequently, the AFM regions are increased while the FM regions are reduced in $Mn_{50}Ni_{40}Sn_{10}$ alloy, which give rise to the considerably large exchange bias effect.[39]

4.4. Magnetoelectric effect

Magnetoelectric (ME) multiferroics, which combine FM and ferroelectric properties in the same system, are particularly appealing for their abundant physical properties and potential applications in devices, such as ME memories, transducers, actuators, and sensors. The ME effects can be classified as direct ME (DME) and converse ME (CME) effects, which are characterized as magnetic-field-induced polarization and electric-field-induced magnetization, respectively. In recent years, laminated ME composites have been extensively investigated owing to their large DME or CME effect.[40] The ME effect in these laminates is the result of the elastic coupling between piezoelectric and magnetostrictive layers, so most studies of the ME composites are focused on the Terfenol-D based laminates for their outstanding magnetostrictive property.[40] However, this rare-earth iron alloy is quite expensive and a fairly large magnetic field is required to obtain a large ME in this composite. Therefore, a ME composite made of a low-cost magnetic alloy and exhibiting a large ME effect is still greatly desired.

Ni–Mn-based FSMAs exhibit a large magnetostrain due to the magnetic field-induced twin boundary motion or magnetic field driven MT.[1–3,8] Based on this effect, these alloys can be utilized as the FM layers of laminated composites to obtain a large DME effect. When an external magnetic field is applied on Ni–Mn-based FSMAs, a large strain is induced and then transferred as a stress in the piezoelectric layer. Finally, a voltage is produced in the ceramic due to the piezoelectric effect. This mechanism has produced large DME effects in Ni_2MnGa/$Pb(Zr_{0.52}Ti_{0.48})O_3$ (PZT), and Ni–Mn–Co–Sn/PZT laminates.[41,42]

As for the CME effect in the laminates composed of magnetostriction alloy and piezoelectric material, the mechanical force (stress) generated from the ceramic is transferred to the magnetic alloy to induce a variation of magnetic flux by the piezomagnetic effect.[43,44] It is known that, in Ni–Mn–Z alloys, the stress can be used as an external force to drive MT, leading to a sharp change of magnetization. Thus, a gi-

ant CME effect can be expected in the FSMAs/piezoelectric laminate.[45] In order to investigate the room-temperature CME effect in Ni–Mn–Z based composite, we first prepared a $Ni_{43}Mn_{41}Co_5Sn_{11}$ (Ni–Mn–Co–Sn) alloy, whose MT temperature is just around 293 K, as shown in Fig. 20. The CME measurement of the Ni–Mn–Co–Sn/PZT laminate was performed by using an induction method.[44] During the measurement, the DC magnetic bias field is applied in the plane of the laminate, and two pickup coils are wrapped around the sample to measure the time dependence of the magnetization in that direction. Figure 21 shows the frequency dependences of the CME coefficients for the composite in different temperatures under an optimum bias magnetic field (H_{bias}) of 660 Oe and an AC electric field of 80 V/mm. At 293 K, giant peak values of CME coefficients are 1.26 G/V, 2.02 G/V, and 2.91 G/V at the frequencies of 8.5 kHz, 52.0 kHz, and 91.5 kHz, respectively, corresponding to the electromechanical resonance frequencies. It is observed that the temperature has an important influence on the CME effect, i.e., the values of CME coefficients at 293 K are much larger than those at 288 K, which can be attributed to the fact that 293 K is very close to the MT temperature and the stress induced magnetic changes are large there. The H_{bias} dependence of CME coefficients at different temperature in an AC electric field of 80 V/mm and 54 kHz is shown

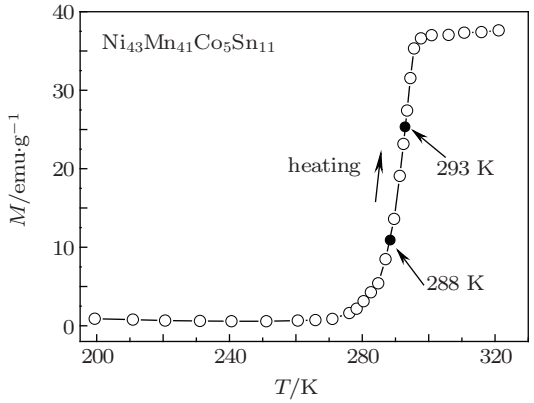


Fig. 20. Thermomagnetization curve for the $Ni_{43}Mn_{41}Co_5Sn_{11}$ alloy under a magnetic field of 1 kOe.[45]

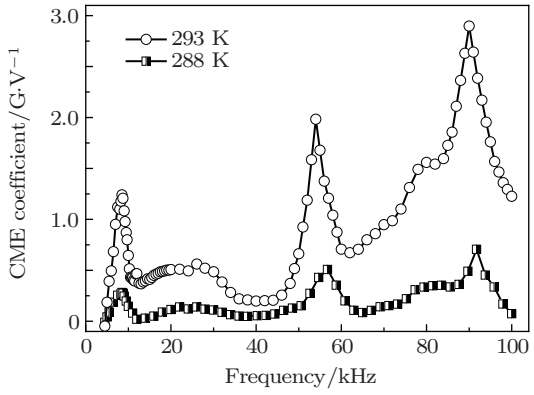


Fig. 21. Frequency responses of CME coefficient at different temperatures with H_{bias} of 660 Oe.[45]

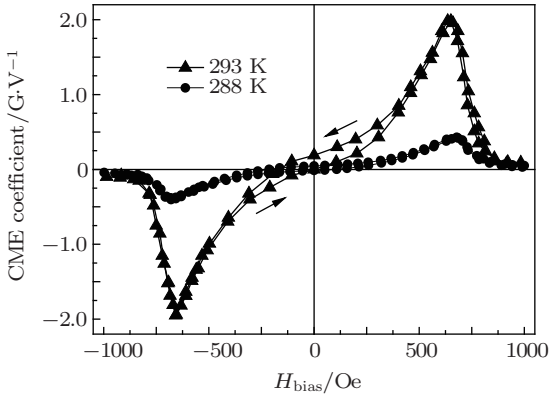


Fig. 22. CME hysteresis loops of the laminated composite at different temperatures.[45]

in Fig. 22. For $T = 293$ K, the CME coefficient increases with the increasing H_{bias} and reaches up to the maximum value of 2.0 G/V at 655 Oe. As mentioned above, the MT can be induced by a magnetic field, i.e., H_{bias}. So the behavior of the CME coefficient is determined by the cooperation of H_{bias} and stress, and the peak at 293 K means that, with the assistance of H_{bias} of 655 Oe, the stress-induced change of magnetization is the largest. Further increasing H_{bias} leads to a decrease of the magnetic change. In the case of 288 K, the value of H_{bias} corresponding to the maximum CME coefficient is 682 Oe, which is somewhat higher than that in 293 K.[45]

5. Conclusion

Ni–Mn–Z (Z = In, Sn, Sb) Heusler alloys are newly discovered FSMAs and have been extensively investigated owing to their abundant physical properties and promising applications in magnetic refrigeration, actuating devices, and sensors. In this review, we have mainly summarized our recent research results about the regulation of MT and the investigation of some related magnetic effects in Ni–Mn–Z FSMAs.

The number of conducting electrons, the distance between Mn atoms, and the relative stability between the parent and the martensitic phases are the main factors for determining the MT in Ni–Mn–Z alloys. Accordingly, some effective methods, such as (i) tuning the composition, (ii) modifying the Mn–Mn distance, and (iii) altering external and internal stresses, are used to adjust the MT in Ni–Mn-based FSMAs.

Due to the special magnetic and crystallographic structures and the strong coupling between magnetism and structure, Ni–Mn–Z FSMAs exhibit a series of interesting magnetic properties, such as magnetocaloric, magnetoresistance, and exchange bias effects. It is known that the MT of these alloys can be driven by an external stress, leading to a large change of magnetization. Based on this distinctive property, giant CME effects are observed in Ni–Mn–Z alloys/PZT laminates, which extends the application area of these magnetic multifunctional materials.

References

[1] Murray S J, Moarioni M, Allen S M, O'Handley R C and Lograsso T A 2000 *Appl. Phys. Lett.* **77** 886

[2] Wang W H, Wu G H, Chen J L, Yu C H, Gao S X, Zhan W S, Wang Z, Gao Z Y, Zheng Y F and Zhao L C 2000 *Appl. Phys. Lett.* **77** 3245

[3] Sozinov A, Likhachev A A, Lanska N and Ullakko K 2002 *Appl. Phys. Lett.* **80** 1746

[4] Hu F X, Shen B G and Sun J R 2000 *Appl. Phys. Lett.* **76** 3460

[5] Sutou Y, Imano Y, Koeda N, Omori T, Kainuma R, Ishida K and Oikawa K 2004 *Appl. Phys. Lett.* **85** 4358

[6] Krenke T, Duman E, Acet M, Wassermann E F, Moya X, Mañosa L and Planes A 2005 *Nat. Mater.* **4** 450

[7] Yu S Y, Liu Z H, Liu G D, Chen J L, Cao Z X, Wu G H, Zhang B and Zhang X X 2006 *Appl. Phys. Lett.* **89** 162503

[8] Kainuma R, Imano Y, Ito W, Sutou Y, Morito H, Okamoto S, Kitakami O, Oikawa K, Fujita A, Kanomota T and Ishida K 2006 *Nature* **439** 957

[9] Planes A, Mañosa L and Acet M 2009 *J. Phys.: Condens. Matter* **21** 233201

[10] Mañosa L, Moya X, Planes A, Gutfleisch O, Lyubina J, Barrio M, Tamarit J L, Aksoy S, Krenke T and Acet M 2008 *Appl. Phys. Lett.* **92** 012515

[11] Wang D H, Zhang C L, Han Z D, Xuan H C, Gu B X and Du Y W 2008 *J. Appl. Phys.* **103** 033901

[12] Han Z D,Wang D H, Zhang C L, Xuan H C, Gu B X and Du Y W 2007 *Appl. Phys. Lett.* **90** 042507

[13] Han Z D, Wang D H, Zhang C L, Xuan H C, Gu B X and Du Y W 2008 *J. Appl. Phys.* **104** 053906

[14] Wang D H, Zhang C L, Xuan H C, Han Z D, Zhang J R, Tang S L, Gu B X and Du Y W 2007 *J. Appl. Phys.* **102** 013909

[15] Han Z D, Chen X, Zhang Y, Chen J, Qian B, Jiang X F, Wang D H and Du Y W 2012 *J. Alloy. Compd.* **515** 114

[16] Aksoy S, Krenke T, Acet M, Wassermann E F, Moya X, Mañosa L and Planes A 2007 *Appl. Phys. Lett.* **91** 241916

[17] Han Z D, Wang D H, Zhang C L, Xuan H C, Zhang J R, Gu B X and Du Y W 2009 *Mater. Sci. Eng. B* **157** 40

[18] Shen J, Gao B, Zhang H W, Hu F X, Li Y X, Sun J R and Shen B G 2007 *Appl. Phys. Lett.* **91** 142503

[19] Xuan H C, Wang D H, Zhang C L, Han Z D, Gu B X and Du Y W 2008 *Appl. Phys. Lett.* **92** 242506

[20] Nayak A K, Suresh K G, Nigam A K, Coelho A A and Gama S 2009 *J. Appl. Phys.* **106** 053901

[21] Mandal K, Pal D, Scheerbaum N, Lyubina J and Gutfleisch O 2009 *J. Appl. Phys.* **105** 073509

[22] Lin H C, Wu S K, Chou T S and Kao H P 1991 *Acta Metall. Mater.* **39** 2069

[23] Piao M, Otsuka K, Miyazaki S and Horikawa H 1993 *Mater. Trans. JIM* **34** 919

[24] Liu Y and Favier D 2000 *Acta Mater.* **48** 3489

[25] Ma S C, Xuan H C, Zhang C L, Wang L Y, Cao Q Q, Wang D H and Du Y W 2010 *Chin. Phys. B* **19** 117503

[26] Llamazares J L S, Sánchez T, Santos J D, Pérez M J, Sanchez M L, Hernando B, Escoda L, Suñol J J and Varga R 2008 *Appl. Phys. Lett.* **92** 012513

[27] Hernando B, Llamazares J L S, Santos J D, Escoda L, Suñol J J, Varga R, Baldomir D and Serantes D 2008 *Appl. Phys. Lett.* **92** 042504

[28] Xuan H C, Xie K X, Wang D H, Han Z D, Zhang C L, Gu B X and Du Y W 2008 *Appl. Phys. Lett.* **92** 102503

[29] Planes A, ObradóE, Gonzàlez-Comas A and Mañosa L 1997 *Phys. Rev. Lett.* **79** 3926

[30] Gonzàlez-Comas A, ObradóE, Mañosa L, Planes A, Chernenko V A, Hattink B J and Labarta A 1999 *Phys. Rev. B* **60** 7085

[31] Cui Y T, Chen J L, Liu G D, Wu G H and Wang W L 2004 *J. Phys.: Condens. Matter* **16** 3061

[32] Ma S C, Xuan H C, Zhang C L, Wang L Y, Cao Q Q, Wang D H and Du Y W 2010 *Appl. Phys. Lett.* **97** 052506

[33] Zhang Q, Cho J H, Li B, Hu W J and Zhang Z D 2009 *Appl. Phys. Lett.* **94** 182501

[34] Rocco D L, Amaral J S, Leitão J V, Amaral V S, Reis M S, Fernandes R P, Pereira A M, Araújo J P, Martins N V, Tavares P B and Coelho A A 2009 *Phys. Rev. B* **79** 014428

[35] Xuan H C, Deng Y, Wang D H, Zhang C L, Han Z D and Du Y W 2008 *J. Phys. D: Appl. Phys.* **41** 215002

[36] Xuan H C, Zheng Y X, Ma S C, Cao Q Q, Wang D H and Du Y W 2010 *J. Appl. Phys.* **108** 103920

[37] Khan M, Dubenko I, Stadler S and AliN 2007 *Appl. Phys. Lett.* **91** 072510

[38] Li Z, Jing C, Chen J P, Yuan S J, Cao S X and Zhang J C 2007 *Appl. Phys. Lett.* **91** 112505

[39] Xuan H C, Cao Q Q, Zhang C L, Ma S C, Chen S Y, Wang D H and Du Y W 2010 *Appl. Phys. Lett.* **96** 202502

[40] Nan C W, Bichurin M I, Dong S X, Viehland D and Srinivasan G 2008 *J. Appl. Phys.* **103** 031101

[41] Zhao K, Chen K, Dai Y R, Wan J G and Zhu J S 2005 *Appl. Phys. Lett.* **87** 162901

[42] Chen S Y, Ye Q Y, Miao W, Wang D H, Wan J G, Liu J M, Du Y W, Huang Z G and Zhou S Q 2010 *J. Appl. Phys.* **107** 09D901

[43] Jia Y M, Or S W, Chan H L W, Zhao X Y and Luo H S 2006 *Appl. Phys. Lett.* **88** 242902

[44] Zhou J P, Guo Y Y, Xi Z Z, Liu P, Lin S Y, Liu G and Zhang H W 2008 *Appl. Phys. Lett.* **93** 152501

[45] Chen S Y, Wang D H, Han Z D, Zhang C L, Du Y W and Huang Z G 2009 *Appl. Phys. Lett.* **95** 022501